Energy levels of CdSe quantum dots: Wurtzite versus zinc-blende structure

H. H. von Grünberg
Department of Physics, Theoretical Physics, University of Oxford, 1 Keble Road, Oxford OX1 3NP, United Kingdom
(Received 13 August 1996)

A simple tight-binding model is used to calculate the energy levels of CdSe quantum dots for two distinct crystal structures: the wurtzite and the zinc-blende structure. Comparison of both level schemes gives an estimate of the shift in energies due to the interior bonding geometry of the lattice structure. Our model makes allowance for the valence-band degeneracy, a finite barrier at the dot boundary, and the full electron-hole interaction. Also calculated are the oscillator strengths of the dipole-allowed transitions. All results are compared with recent experimental findings. [S0163-1829(97)05303-4]

I. INTRODUCTION

The energies of electron-hole states in nanometer-size semiconductor quantum dots[1] can be regarded as made up from two contributions, the electron-hole interaction energy and an energy contribution that is due to the confinement.[2,3] While the confinement energy dominates in very small dots with a radius R appreciably smaller than the bulk exciton radius (strong-confinement regime), the attractive Coulomb interaction between hole and electron becomes the more important of the two in the weak-confinement regime, when the dot radius sufficiently exceeds the exciton radius, and will lead to the formation of the familiar bulk excitons in the limit $R\rightarrow\infty$. Quantum dots in both size regimes have been the subject of numerous theoretical papers[4] and various aspects of this problem have been studied. We mention just a few of them: While in early works[2,3,5–9] the problem has been tackled with a simple two-band model based on the effective-mass approximation (EMA), a multiband approach has been made in more recent studies[12–18] to take account of the valence-band degeneracy. This has been done either by resorting again to the EMA,[12,13] or, alternatively, by choosing a tight-binding approach.[14–18] Both methods are thoroughly compared in Ref. 18. Other aspects of the problem are the dielectric mismatch at the dot boundaries,[3,8] the presence of an external magnetic[10] or electric[11] field, and the significance of confinement potentials that allow for finite barriers at the dot boundary.[17,19]

In a recent absorption experiment on CdSe quantum dots, Norris *et al.*[20] have been able to observe not only the electron-hole ground state but also a series of higher excited states. They measured the size dependence of the levels for dots in the strong-confinement regime (between 19 and 115 Å diameter) and analyzed their data using a theoretical calculation made by Ekimov *et al.*[13] In this theory, special account was taken of the valence-band degeneracy and the nonparabolicity of the conduction band, but the electron-hole interaction was approximated very crudely by a constant. Also, these theoretical curves have been calculated for a dot-size range different from that range actually studied in the experiment so that the experimental data for the smaller sized dots have not yet been theoretically evaluated.

In this paper we repeatedly refer to this experiment, for three reasons. The first is the obvious one and relates to the questions left unanswered by the analysis of this experiment: Can the levels of the smaller dots be equally well explained with the simple valence-band model applied in Ref. 13? How important is the electron-hole interaction, is it allowed to take this as a constant in the strong confinement regime? How can the as yet unexplained ground-state energies be theoretically interpreted?

The second reason why these experimental results might be worth reconsidering is that the newly observed higher excited states furnish an invaluable testing ground for theoretical predictions, which so far could only be checked with respect to ground-state data, such as, for instance, the effect of a finite barrier at the dot boundary. Such a barrier has proven to be essential in the case of CdS quantum dots,[17] and it is therefore reasonable to assume that it is also important in the CdSe system where it can be expected to provide the missing link required to settle the open question of the ground-state energies.

However, it is mainly a puzzling inconsistency found in the experimental work of Shiang *et al.*[21] that has led us to analyze the data of Norris *et al.* again. According to the theory of Ekimov *et al.*. one would expect triply degenerate states to occur (corresponding to the irreducible representation T), while the Raman depolarization data of Shiang *et al.* have clearly shown that only states of the one- and two-dimensional representations A and E but not of the three-dimensional representation T are present. A possible source of this apparent discrepancy might be the wurtzite structure of the CdSe crystal, which corresponds to a point symmetry group that simply does not possess a three-dimensional irreducible representation. Using a theory where the lattice structure is neglected and replaced by a continuum, the triply degenerate states would therefore split into A and E states when the lattice symmetry is properly taken into account. Thus the main question to be addressed in this paper is: What energetic effect is brought about by the interior bonding geometry of the lattice structure?

Not only is this question relevant to finding a consistent description for both of the aforementioned experiments, but it is also of some consequence for the tight-binding models and in particular the effective-bond-orbital method (EBOM) introduced by Chang[22] that have been used repeatedly for calculating the energy levels in quantum dots.[14–18] All of these models are based on the same *ad hoc* assumption origi-

nally made by Chang that the exact lattice structure is unimportant and that it can thus be replaced by an fcc lattice that is easier to treat. By calculating the energy shifts induced by the lattice structure in the prototypical CdSe system, we can estimate the error produced by this assumption.

The strategy pursued in this paper to answer these questions is to compare two calculations, both based on a simple tight-binding model (basically the same as in Refs. 16–18,22 and 23), but taking the lattice to be of the wurtzite structure in the one case and of the zinc-blende structure in the other. The difference in the results of both calculations will then reveal the energetic effect of the discrete lattice, and comparison can be made with the experimental data of Norris *et al.*

II. THEORY

A. The Schrödinger equation for an electron-hole pair in a quantum dot

To calculate the energy levels of an electron-hole pair in a quantum dot, one has to consider the effect of confinement and electron-hole interaction on the otherwise free hole and electron states. For the CdSe dot, these are derived as follows: for the hole, from one of the six spin-orbit split valence bands and for the electron from the *s*-like conduction band. With the Hamilton operators $\mathcal{H}_h$ and $\mathcal{H}_e$ for the non interacting pair, $\mathcal{V}_{eh}(r_{eh})=-e^2/\epsilon r_{eh}$ for their statically screened Coulomb interaction and $\mathcal{V}_e(\vec{r}_e)$, $\mathcal{V}_h(\vec{r}_h)$ for the confinement potentials, the Schrödinger equation assumes the form

$$[\mathcal{H}_h+\mathcal{H}_e+\mathcal{V}_{eh}(r_{eh})+\mathcal{V}_e(\vec{r}_e)+\mathcal{V}_h(\vec{r}_h)]|\lambda\rangle=E_\lambda|\lambda\rangle. \quad (1)$$

Both the zinc-blende and the wurtzite structure can be regarded as consisting of two interpenetrating lattices (one for each kind of atom) displaced along the body diagonal of the cubic cell by one quarter the length of the diagonal $[\vec{R}_D=a/4\,(1,1,1)]$. They differ in their type of sublattice, which is fcc in the zinc blende and hcp in the wurtzite form. If we disregard all other bands and restrict our consideration exclusively to the six valence bands and the one conduction band (which can be thought of as arising from the corresponding atomic *p* levels of the Se atoms and *s* levels of the Cd atoms), then hole and electron are each confined to one sublattice. In other words, the symmetry for $\mathcal{H}_h$ and $\mathcal{H}_e$ in Eq. (1) is purely fcc or hcp, which is then, on introducing the confinement potentials, further reduced to the point group O_h or D_{3h}, respectively, for the operators $[\mathcal{H}_h+\mathcal{V}_h(\vec{r}_h)]$ and $[\mathcal{H}_e+\mathcal{V}_e(\vec{r}_e)]$. In this approximation the two sublattices are not coupled until the electron-hole interaction is switched on. However, since this is a small perturbation in the strong-confinement regime considered here, the solutions to Eq. (1) may still be discussed in terms of the symmetry of the underlying sublattices.

The eigenvalues and eigenvectors of Eq. (1) can be found numerically once it is transformed into a system of algebraic equations. To do this, we need to define a set of basis states, conveniently one that is chosen in accordance with the symmetry of the problem: Denoting the creation operator of a conduction-band electron (spin σ_e) at the lattice site $\vec{R}_e$ by $b^\dagger_{\vec{R}_e\sigma_e}$, and that of the valence-band hole at $\vec{R}_h$ by $a^\dagger_{\vec{R}_hp\sigma_h}$ (angular momentum and spin quantum numbers $p=p_x,p_y,p_z$ and σ_h), we first introduce the states

$$|\vec{R}_hp\sigma_h\rangle=a^\dagger_{\vec{R}_hp\sigma_h}|0\rangle,$$

$$|\vec{R}_e\sigma_e\rangle=b^\dagger_{\vec{R}_e\sigma_e}|0\rangle, \quad (2)$$

in terms of which the symmetry-adapted basis is to be expressed. $|0\rangle$ is the vacuum state consisting of completely filled valence and empty conduction bands. The states (2) are taken to be orthogonal to each other. From these states, new hole states may be formed,

$$|U_h\Gamma_hi\mu\rangle=\sum_{\vec{R}_h(U_h),p,\sigma_h}A(U_h\Gamma_hi\mu;\vec{R}_hp\sigma_h)|\vec{R}_hp\sigma_h\rangle, \quad (3)$$

transforming according to the *i*th row of the irreducible representation Γ_h of the double point groups O_h^* or D_{3h}^* where $i=1,\ldots,d_{\Gamma_h}$ with d_{Γ_h} for the dimension of Γ_h. The sum is over all lattice vectors $\vec{R}_h$ belonging to the same subshell U_h, where the term ''subshell'' refers to a subset of lattice vectors of a shell. While a shell consists of all vectors having the same distance from the origin, a subshell comprises those vectors within a shell that span a subspace that is invariant under all operations of the point group of the lattice. μ is the multiplicity index that (for a given subshell) distinguishes the states belonging to the same symmetry species.

From the electron expression equivalent to Eq. (3), we retain only those states that transform like the totally symmetric representation A_{1g} (Γ_1) of O_h (D_{3h}). With $N(U_e)$ as an abbreviation for the number of sites on the subshell U_e, these are the states:

$$|U_e\Gamma_e\sigma_e\rangle=\frac{1}{\sqrt{N(U_e)}}\sum_{\vec{R}_e(U_e)}|\vec{R}_e\sigma_e\rangle. \quad (4)$$

Because the spin transforms like the E_g' (Γ_7) representation of the O_h^* (D_{3h}^*) group, Γ_e can only be the E_g' (Γ_7) representation. A multiplicity index, such as μ in Eq. (3), is now dispensable because for each subshell there is by definition exactly one totally symmetric state. Of these states, just one particular linear combination, namely,

$$|\lambda^e_{1s}\Gamma_e\sigma_e\rangle=\sum_{U_e}C(U_e)|U_e\Gamma_e\sigma_e\rangle, \quad (5)$$

is of interest to us. This is the ground state (energy ϵ_{1s}) of the electron in the confinement potential, i.e., the ground state for the reduced problem where in the Schrödinger Eq. (1) only $\mathcal{H}_e$ and $\mathcal{V}_e(\vec{r}_e)$ are retained. This step of taking account merely of the ground state and discarding all higher states in the discrete level scheme of the confined electron represents our main approximation for solving Eq. (1). It is made for the obvious reason of reducing the overall number of states, and will be justified in Sec. III.

The basis that is to be used for Eq. (1) can now be defined to be the product states of Eqs. (3) and (5),

$$|U_h\Gamma_hi\mu\rangle|\lambda^e_{1s}\Gamma_e\sigma_e\rangle. \quad (6)$$

Only the indices U_h and μ are variable here while the set $(\Gamma_h i\Gamma_e\sigma_e)$ specifies the symmetry of the electron-hole pair considered and is fixed for each calculation. Considering the spatial dimensions to be so small that the field acting on it can be taken to be uniform over the unit cell of the crystal, we may write the interaction operator $\mathcal{V}_{eh}(r_{eh})$ between these basis states approximately in the form

$$-\frac{e^2}{\epsilon}\langle U_h'\Gamma_h i\mu'|\langle\lambda_{1s}^e\Gamma_e\sigma_e|\frac{\delta_{\vec{R}_e\vec{R}_e'}\delta_{\vec{R}_h\vec{R}_h'}}{|\vec{R}_h-\vec{R}_e|}|\lambda_{1s}^e\Gamma_e\sigma_e\rangle \times|U_h\Gamma_h i\mu\rangle=-\frac{e^2}{\epsilon}\delta_{U_h'U_h}\delta_{\mu'\mu}P(U_h) \tag{7}$$

with

$$P(U_h)=\sum_{U_e,\vec{R}_e(U_e)}\frac{|C(U_e)|^2}{N(U_e)}\frac{1}{|\vec{R}_{U_h}-\vec{R}_e|}, \tag{8}$$

where $\vec{R}_{U_h}$ is any one of the vectors $\vec{R}_h$ of the subshell U_h. Similarly, we also assume that the hole confinement potential $\mathcal{V}_h(\vec{r}_h)$ of Eq. (1) is purely diagonal in this basis with diagonal elements given by $V_h(\vec{R}_{U_h})=V_h(U_h)$. Since the electron-hole interaction is but a minor correction to the energies compared to the effect of the confinement, the approximations thus made are certainly very good. Note that we need not bother about $\vec{R}_{U_h}$ becoming $\vec{R}_e$ in Eq. (8) on the grounds that with the electron and hole confined each to one sublattice, they cannot come closer than $\vec{R}_D$.

Expressing Eq. (1) in terms of the basis (6), we arrive at an eigenvalue equation,

$$\sum_{U_h'\mu'(U_h')}\left\{\left(\epsilon_{1s}-\frac{e^2}{\epsilon}P(U_h)+V_h(U_h)\right)\delta_{U_hU_h'}\delta_{\mu\mu'} +\langle U_h\Gamma_h i\mu|\mathcal{H}_h|U_h'\Gamma_h i\mu'\rangle\right\}c(\lambda\Gamma_h i\Gamma_e\sigma_e;U_h'\mu') =E_\lambda c(\lambda\Gamma_h i\Gamma_e\sigma_e;U_h\mu), \tag{9}$$

from which — for an electron-hole pair of given symmetry $(\Gamma_h i\Gamma_e\sigma_e)$ — we can calculate the energy levels E_λ and the expansion coefficients for the final states,

$$|\lambda\Gamma_h i\Gamma_e\sigma_e\rangle=\sum_{U_h\mu(U_h)}c(\lambda\Gamma_h i\Gamma_e\sigma_e;U_h\mu)|U_h\Gamma_h i\mu\rangle \times|\lambda_{1s}^e\Gamma_e\sigma_e\rangle. \tag{10}$$

Equation (9) is a system of equations whose dimension is given by the number of subshells taken into account. For all confinement potentials other than hard wall potentials the radius of the outer subshell should considerably exceed the radius defining the quantum dot in order to avoid artificial size effects. Hard-wall potentials, on the other hand, can most easily be realized by simply choosing the number of subshells in consistency with the size of the quantum dot.

B. The tight-binding model

It remains to be explained how the matrix elements $\langle\vec{R}_e'\sigma_e'|\mathcal{H}_e|\vec{R}_e\sigma_e\rangle$ and $\langle\vec{R}_h'p'\sigma_h'|\mathcal{H}_h|\vec{R}_hp\sigma_h\rangle$ [and thus — through the transformation (3) — $\langle U_h'\Gamma_h i\mu'|\mathcal{H}_h|U_h\Gamma_h i\mu\rangle$] are obtained from the band structure of the crystal. For the fcc lattice — which we first concentrate on — this has been described in detail several times before.[16,17,22,23] We therefore discuss merely the case of the s-like conduction band $E_s(\vec{k})$ in order to just give an idea of how to derive transfer elements in $\vec{R}$ from band-structure data, and leave it at a brief outline for the more complicated case of the valence bands.

$E_s(\vec{k})$ has its band extremum at $\vec{k}=0$. Whatever might be its true shape in the entire Brillouin zone, in the vicinity of $\vec{k}=0$, $E_s(\vec{k})$ can always be approximated by the nearest-neighbor tight-binding expression[24]

$$E_s(\vec{k})\approx E^{\mathrm{tb}}(\vec{k})=4t(3-c_xc_y-c_xc_z-c_yc_z), \tag{11}$$

with $c_i=\cos(k_ia/2)$ $(i=x,y,z)$ and the fcc lattice constant a, provided only that we choose t to be equal to $\hbar^2/(2m^*a^2)$. For then $E^{\mathrm{tb}}(\vec{k})$ will have the same curvature at $\vec{k}=0$ as $E_s(\vec{k})$, namely, that encoded by the effective mass m^*. We know, on the other hand, that in the original tight-binding theory[24] t is the transfer-matrix element $E_{ss}(110)$ between s orbitals at adjacent fcc lattice sites, which, in our notation, is $\langle\vec{R}_e'\sigma_e|\mathcal{H}_e|\vec{R}_e\sigma_e\rangle$ when $\vec{R}_e'-\vec{R}_e$ is one of the nearest-neighbor lattice sites $\vec{R}_{nn}$. Hence we see that by choosing

$$\langle\vec{R}_e'\sigma_e'|\mathcal{H}_e|\vec{R}_e\sigma_e\rangle=\frac{\hbar^2}{2m^*a^2}\delta_{\vec{R}_e'-\vec{R}_e,\vec{R}_{nn}}\delta_{\sigma_e',\sigma_e}$$

we have determined the matrix elements in $\vec{R}$ space in such a way that they are consistent with the band near $\vec{k}=0$.

With an appropriate choice of the zero of energy, the whole Hamilton matrix for an electron in the dot becomes

$$\langle\vec{R}_e'\sigma_e'|\mathcal{H}_e+\mathcal{V}_e(\vec{r}_e)|\vec{R}_e\sigma_e\rangle \approx\{[12t+V_e(\vec{R}_e)]\delta_{\vec{R}_e'\vec{R}_e}-t\,\delta_{\vec{R}_e'-\vec{R}_e,\vec{R}_{nn}}\}\delta_{\sigma_e'\sigma_e}, \tag{12}$$

which when transformed according to Eq. (4) and diagonalized, then provides us with both the energy ϵ_{1s} used in Eq. (9) and the coefficients $C(U_e)$ of Eq. (5).

For the valence bands, one pursues the same strategy, though this time the fourfold degeneracy of the bands at $\vec{k}=0$ requires the simple effective mass m^* to be replaced by a mass tensor of rank 4, whose elements may be brought into correspondence with the set of Luttinger parameters[25] $\gamma_1,\gamma_2,\gamma_3$. These parameters, along with the constant α from the spin-orbit (SO) splitting at the center of the Brillouin zone, can now be used in a tight-binding expression, just as in Eq. (11), to give an approximate description of the whole valence-band structure. From this expression, one then obtains the connection between the Luttinger parameter and the nearest-neighbor tight-binding parameters[24] $E_{xx}(110)$, $E_{xy}(110)$, and $E_{xx}(011)$ (Refs. 22 and 23). In the original tight-binding theory, these three quantities are transfer-

matrix elements in a $\vec{R}$ basis, a fact that suggests their use as an approximation for the matrix element $\langle \vec{R}_h' p' \sigma_h' | \mathcal{H}_h | \vec{R}_h p \sigma_h \rangle$. In this way, one has again determined the matrix elements in $\vec{R}$ from the data of the band structure at $\vec{k}=0$, which this time are the Luttinger parameters and the SO constant α. One finds

$$\begin{aligned}\langle \vec{R}_h' p' \sigma_h' | \mathcal{H}_h | \vec{R}_h p \sigma_h \rangle &\approx [V^0 \delta_{p'p} \delta_{\sigma_h' \sigma_h} + V^{SO}(p' \sigma_h'; p \sigma_h)] \delta_{\vec{R}_h' \vec{R}_h} \\ &+ D(\vec{R}_h' p'; \vec{R}_h p) \delta_{\vec{R}_h' - \vec{R}_h, \vec{R}_{nn}} \delta_{\sigma_h' \sigma_h}, \end{aligned} \tag{13}$$

where V^0 is a constant chosen to bring the zero of energy to lie at the top of the valence bands and $V^{\mathrm{SO}}(p'\sigma_h'; p\sigma_h)$ an element of the ordinary 6×6 SO matrix depending solely on α and constructed in such a way that its eigenvalues are α and -2α. The elements $D(\vec{R}_h' p'; \vec{R}_h p)$ of the matrix $\underline{\underline{D}}(\vec{R}_{nn})$ can be obtained either directly from the parameters $E_{xx}(110)$, $E_{xy}(110)$, and $E_{xx}(011)$ with the help of simple symmetry considerations, or, in a less accurate approximation, through appropriate rotations of the p orbitals by means of the integrals $pp\sigma$ and $pp\pi$, to which $E_{xx}(110)$, $E_{xy}(110)$, and $E_{xx}(011)$ reduce in going from the three-center to the two-center approximation:[24]

$$\begin{aligned} E_{xx}(110) &= \tfrac{1}{2}(pp\sigma + pp\pi), \\ E_{xx}(011) &= pp\pi, \\ E_{xy}(110) &= \tfrac{1}{2}(pp\sigma - pp\pi). \end{aligned} \tag{14}$$

In this latter case the elements $D(\vec{R}_h' p'; \vec{R}_h p)$ are given by

$$\underline{\underline{D}}(\vec{R}_{nn}) = \underline{\underline{R}}^{-1}(\vec{R}_{nn}) \begin{pmatrix} pp\sigma & & \\ & pp\pi & \\ & & pp\pi \end{pmatrix} \underline{\underline{R}}(\vec{R}_{nn}), \tag{15}$$

where $\underline{\underline{R}}(\vec{R}_{nn})$ is a matrix rotating the Hamilton matrix from a coordinate system whose z axis is directed along $\vec{R}_{nn}$ to a space-fixed one. To determine $pp\sigma$ and $pp\pi$, we invert Eq. (14) to find

$$\begin{aligned} pp\sigma &= E_{xx}(110) + E_{xy}(110), \\ pp\pi &\approx \tfrac{1}{2} E_{xx}(011) + \tfrac{1}{2}[E_{xx}(110) - E_{xy}(110)], \end{aligned} \tag{16}$$

where for $pp\pi$ a further approximation was made whose consequences will be discussed in Sec. III.

The quantities $pp\sigma$ for the valence bands and t [or $E_{ss}(110)$] for the conduction band can be interpreted as effective σ bonds, and, similarly, $pp\pi$ as a π bond. Now the essential idea of this paper is to model not only the zinc blende but also the wurtzite form of CdSe crystals with the help of these effective bonds; i.e., we use the *same* bonds — originally derived only for zinc-blende CdSe — also for the wurtzite form and change in Eqs. (9), (12), (13), and (15) only the underlying lattice from fcc to hcp. This approximation means in k space that we assume the CdSe crystal to have the same band structure at the center of the Brillouin zone for both crystal structures (described by m^*, the SO constant α, and the Luttinger parameters of the zinc-blende structure). We thereby neglect a small difference in the conduction-band effective masses for both structures and, more importantly, an additional crystal-field splitting of 26 meV of the valence bands at $\vec{k}=0$ in the wurtzite structure. Compared to the calculated electron-hole pair energies, this splitting energy may, however, be regarded as negligible. In making this approximation, we focus solely on the energetic effect brought about by the differently shaped Brillouin zones, or, in other words, by the different interior bonding geometry.

In both lattices, there are 12 nearest-neighbor sites. Assuming the ideal c/a ratio for the hcp lattice, nine sites are identical. The sets of the three remaining sites are connected with each other by a rotation through 180° along the c axis of the hcp lattice. Notice that the calculation of the matrices $\underline{\underline{D}}(\vec{R}_{nn})$ using the two-center parameters in Eq. (15) is possible for both lattices, while the fcc symmetry is required in the case where these matrices are set up with the three-center parameters.

C. Oscillator strength and symmetry reduction

We next discuss how to determine the oscillator strengths $f(E_\lambda)$ for a transition from the ground state to the level E_λ of Eq. (9). We start from the expression

$$f(\hbar\omega) \sim \sum_f |\langle \psi_f | T \psi_i \rangle|^2 \delta(E_f - E_i - \hbar\omega) \tag{17}$$

for a dipole-allowed transition (operator T) from the initial state ψ_i to the final states $|\psi_f\rangle$, which in our case is the state $|\lambda \Gamma_h i \Gamma_e \sigma_e\rangle$ that we have calculated in Eq. (10). Expressed through the creation operators introduced in (2), $|T\psi_i\rangle$ takes on the form

$$|T\psi_i\rangle = \sum_{U, \vec{R}(U)} \delta_{\sigma_e \sigma_h} a^\dagger_{\vec{R} p_{pol} \sigma_h} b^\dagger_{\vec{R} \sigma_e} |0\rangle, \tag{18}$$

and describes a transition proportional to the probability that electron and hole are at the same site. Since in a finite-size quantum dot, it is pointless to introduce relative electron-hole coordinates r_{eh}, as usually done for an exciton in a crystal, the single term of the probability amplitude for $r_{eh}=0$ used in exciton theory must now be replaced by a sum of these amplitudes over all sites. p_{pol} is p_x, p_y, or p_z depending on the polarization of the exciting light. From this equation along with the Eqs. (2), (3), (4), (5), and (10), one then finds

$$\begin{aligned} \langle \psi_f | T \psi_i \rangle &= \sum_{U, \vec{R}(U), \mu(U)} c(\lambda \Gamma_h i \Gamma_e \sigma_e; U \mu) \\ &\quad \times A(U \Gamma_h i \mu; \vec{R} p_{\mathrm{pol}} \sigma_e) \frac{C(U)}{\sqrt{N(U)}} \\ &= K(\lambda \Gamma_h i \Gamma_e \sigma_e p_{\mathrm{pol}}), \end{aligned} \tag{19}$$

so that Eq. (17) after averaging over both spin directions, becomes

$$f(E_\lambda)=\frac{1}{2}\sum_{i,\sigma_e}|K(\lambda\Gamma_h i\Gamma_e\sigma_e p_{\rm pol})|^2, \tag{20}$$

where E_i is set equal to zero. For unpolarized light this expression has to be averaged over the three $p_{\rm pol}$ directions.

The last few equations help establish the selection rules. The O_h^* group possesses the double-valued irreducible representation $E_g',E_u',E_g'',E_u'',U_g',U_u'$ plus the single-valued representations $A_{1g},A_{1u},A_{2g},A_{2u},E_g,E_u,T_{1g},T_{1u},T_{2g},T_{2u}$, while the D_{3h}^* group (isomorph to the D_6 group) has $\Gamma_7,\Gamma_8,\Gamma_9$ and A_1', A_1'', A_2', A_2'', E', E'' as double- and single-valued representations, respectively. The three p orbitals transform as T_{1u} for the O_h^* group and as $A_2''+E'$ for D_{3h}^* (A_2'' for p_z) so that state (18) transforms as $A_{1g}\times T_{1u}\times E_g'\times E_g'$ or $A_1'\times(A_2''+E')\times\Gamma_7\times\Gamma_7$ while the final states $|\lambda\Gamma_h i\Gamma_e\sigma_e\rangle$ carry the representation $\Gamma_h\times E_g'$ or $\Gamma_h\times\Gamma_7$ [Γ_e is either E_g' or Γ_7, see Eq. (4)]. From this, we easily infer (i) that for the D_{3h}^* group, Γ_h can only be Γ_8 if z-polarized light is used, and either Γ_8 or Γ_9 for unpolarized light, but never Γ_7 ($A_2''\times\Gamma_7=\Gamma_8$, $E'\times\Gamma_7=\Gamma_8+\Gamma_9$), and (ii) that for the O_h^* group, Γ_h must be either the E_u' or the U_u' representation, irrespective of the polarization direction. In view of these selection rules, we henceforth consider only the representations Γ_8, Γ_9, E_u' and U_u' for Γ_h. Finally, the overall symmetry of the electron-hole pair can be found from the reduction of the product $\Gamma_h\times\Gamma_e$:

$$\begin{aligned}
U_u'\times E_g'&=E_u+T_{1u}+T_{2u},\\
E_u'\times E_g'&=A_{1u}+T_{1u},\\
(\Gamma_8+\Gamma_9)\times\Gamma_7&=E'+(A_2''+E')+(A_1''+E''),\\
\Gamma_8\times\Gamma_7&=A_1''+(A_2''+E').
\end{aligned}\tag{21}$$

Returning to Eq. (3), we close this section by answering the question of how to determine the coefficients $A(U_h\Gamma_h i\mu;\vec{R}_h p\sigma_h)$, i.e., how to combine the states $|\vec{R}_h p\sigma_h\rangle=|\vec{R}_h\rangle|p\sigma_h\rangle$ of a given subshell U_h so that they transform like Γ_h. The most convenient strategy is to look separately for the superpositions of $|\vec{R}_h\rangle$ and $|p\sigma_h\rangle$ that transform according to the irreducible representations Γ_R and Γ_p, respectively, and then to determine the linear combinations of $|\vec{R}_h\rangle|p\sigma_h\rangle$ from the evaluation of $\Gamma_R\times\Gamma_p$. To elaborate on this, let us focus on the hcp lattice for a moment. Γ_p is then Γ_8 or Γ_9 and the states are ($|81\rangle$ short for $|\Gamma_8,1\rangle$)

$$\begin{aligned}
&|81\rangle=|p_z\downarrow\rangle,\quad |82\rangle=|p_z\uparrow\rangle,\quad |81\rangle=|p_+\downarrow\rangle,\\
&|82\rangle=|p_-\uparrow\rangle,\quad |91\rangle=|p_+\uparrow\rangle,\quad |92\rangle=|p_-\downarrow\rangle,
\end{aligned}\tag{22}$$

[$p_\pm=(p_x\pm ip_y)/\sqrt{2}$] where the first two states stem from $A_2''\times\Gamma_7$ and the remainder from $E'\times\Gamma_7$. In Ref. 26, a simple computational procedure is described as to how to find the linear combinations of $|\vec{R}_h\rangle$ for the Γ_R representation. We denote these new states by $|A_1'\rangle$, $|A_1''\rangle$, $|A_2'\rangle$, $|A_2''\rangle$ for the one-dimensional representations of D_{3h} and by $|E',1\rangle$, $|E',2\rangle$, $|E'',1\rangle$, $|E'',2\rangle$ for the two-dimensional ones. The latter are combined to give $|\pm 1'''\rangle=(|E'''',1\rangle\pm i|E'''',2\rangle)/\sqrt{2}$. From the products of these states and the states in Eq. (22), we may now form the states for Γ_h we were looking for. They are

$$\begin{aligned}
&|81\rangle|A_1'\rangle,\quad |81\rangle|A_2'\rangle,\quad |92\rangle|-1'\rangle,\\
&|82\rangle|+1''\rangle,\quad |91\rangle|-1''\rangle
\end{aligned}$$

for the case $\Gamma_h=\Gamma_8$, and

$$\begin{aligned}
&|91\rangle|A_1'\rangle,\quad |92\rangle|A_1''\rangle,\quad |91\rangle|A_2'\rangle,\quad |92\rangle|A_2''\rangle,\\
&|82\rangle|-1''\rangle,\quad |81\rangle|+1''\rangle
\end{aligned}$$

for $\Gamma_h=\Gamma_9$. Only the first of the two possible states is given. For the O_h^* group and the fcc lattice, the equivalent information can be found elsewhere.[22,23]

III. RESULTS AND DISCUSSION

Now that we have outlined its theoretical background, we are equipped to give the details of the calculation. This is performed in five steps, which are (i) diagonalizing the Hamilton matrix (12) for an electron in the dot (with $a=6.052$ Å and $m^*=0.11$ from Ref. 27 for lattice constant and conduction-band effective-mass) to determine $C(U_e)$ and ϵ_{1s}, (ii) using $C(U_e)$ for evaluating the hole potential, Eq. (8) [with the static dielectric constant $\epsilon=6.1$ (Ref. 27)], (iii) setting up the hole matrix, Eq. (13) (with the constant $3\alpha=0.42$ eV (Ref. 27) for the valence-bands SO splitting and the Luttinger parameters γ_1, γ_2, γ_3), (iv) solving Eq. (9) for each allowed Γ_h to find $c(\lambda\Gamma_h i\Gamma_e\sigma_e;U_h\mu)$ and E_λ, and finally (v) using $c(\lambda\Gamma_h i\Gamma_e\sigma_e;U_h\mu)$ to calculate f values from Eq. (20) to weed out all levels with oscillator strengths below a certain threshold value ($f_T=0.05$). This calculation cycle is then repeated for various dot radii R where the radius of a spherical quantum dot is computed by $R=(3N/16\pi)^{1/3}a$ from the number N of sites in the dot. In the choice of the Luttinger parameters we follow Ekimov *et al.*[13] who could successfully explain their absorption measurements on CdSe quantum dots using $\gamma_1=2.1$ and $\gamma_2=\gamma_3=0.55$.

We first focus on the case of a fcc lattice for which Fig. 1 shows the energy levels as a function of the dot size. An experimentally accessible range of dot radii is chosen. The levels are obtained from Eq. (9) for hard-wall confinement potentials. Figures 1(a), 1(b), and 1(c) differ in the potential $P(U_h)$ which is switched off [$P(U_h)=0$ for all U_h] in Figs. 1(a) and 1(b). The levels displayed in Figs. 1(a), and 1(b) are then simply the hole energy levels (with $\epsilon_{1s}=0$ being set to zero), i.e., the eigenvalues of hole band matrix $\langle U_h\Gamma_h i\mu|\mathcal{H}_h|U_h'\Gamma_h i\mu'\rangle$.

Figure 1(a) gives the first 14 hole levels of E_u' — and U_u' — symmetry for a sequence of various dot radii. Owing to the confinement, the average spacing between the levels grows with decreasing R. They start off from their asymptotical values of the band states of the unconfined crystal, the higher ones from the top of the $j=3/2$ valence bands, the lower ones from the $j=1/2$ band (split-off band). Those levels involved in transitions with a f value greater than f_T are marked by an additional symbol. In this way, a subset of

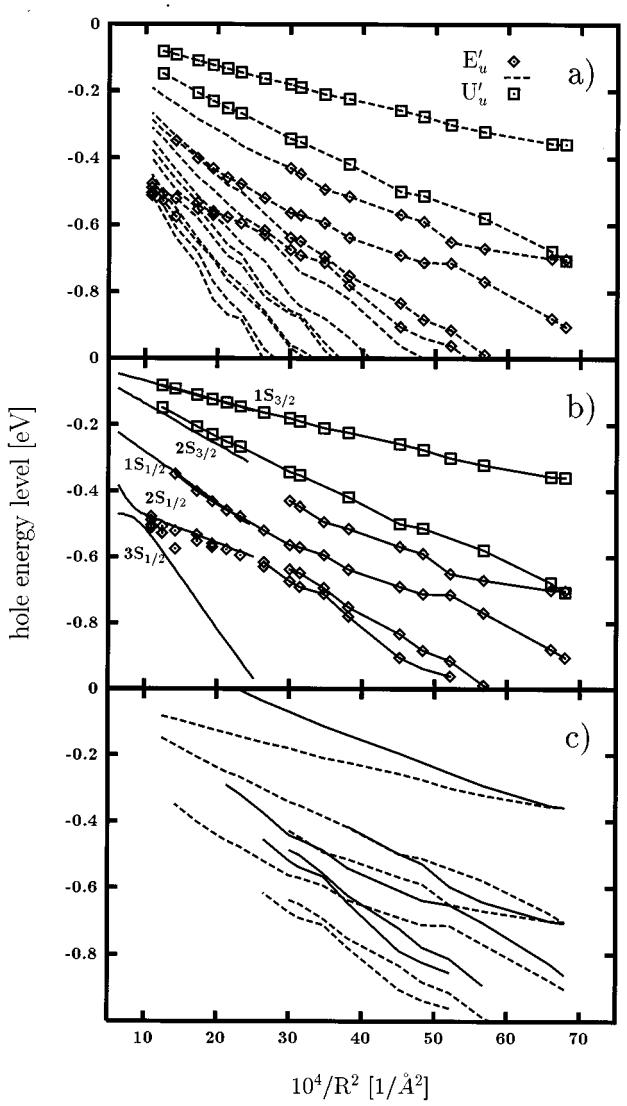

FIG. 1. Hole energy levels of CdSe quantum dots for various dot radii without (a), (b), and with (c) electron-hole interaction. (a) First 14 allowed levels, connected to give continuous lines (dashed lines). Additional symbols for levels involved in transitions with sufficiently high oscillator strengths ($f > f_T$). (b) Comparison of levels where $f > f_T$ with theoretical results of Ekimov *et al.* (Ref. 13) (c) Effect of the electron-hole interaction. Dashed lines are for the level structure of (b). To facilitate easy comparison, energies have been shifted by 200 meV. Note that since the levels are plotted over $1/R^2$, the zero of the x axis corresponds to the case of no confinement.

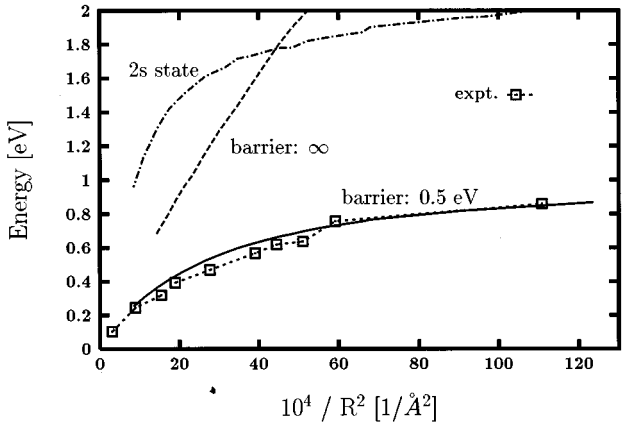

FIG. 2. Size dependence of the ground-state energy of an electron-hole pair in a CdSe quantum dot as calculated from Eq. (9). Comparison between dashed and solid lines reveals the effect of a finite barrier at the dot boundary. Experimental data from Norris *et al.* (Ref. 20) is shown. Also shown is the transition energy to the $2s$ electron level.

levels observable in an experiment can be extracted from the vast number of eigenvalues of the hole matrix. They are compared in Fig. 1(b) with the levels of Ekimov *et al.* based on exactly the same input parameters, yet calculated in a continuum theory. The latter are marked in the plot by the notation[13] Q_F where F is the total momentum of the state and Q the momentum of the envelope function, giving a symmetry classification that is obviously compatible to our ($S_{1/2} \rightarrow A_{1g} \times E'_u = E'_u$ and $S_{3/2} \rightarrow A_{1g} \times U'_u = U'_u$).

The main difference between a continuum based theory and a discrete lattice theory is that the first always assumes an infinite number of states to be present, irrespective of the actual size of the dot (infinite width of the energy spectrum), while a discrete-lattice theory correctly takes account of the fact that with decreasing dot size there are fewer states available, which are distributed over a finite and size-independent energy range. Accordingly, both theories differ less for larger dots with a greater extension to the wave function under consideration. This explains why in Fig. 1(b) there is virtually no difference between the two theories for the highest hole level (having the most extended wave function). However, they must necessarily differ for the deeper levels having wave functions with growing short-wavelength contributions. This can already be observed in the range $10^4/R^2 < 25/\text{Å}^2$ in Fig. 1(b) where the deviations (though still small) are most prominent between the $3S_{1/2}$ and the lowest E'_u level. Resulting from the discreteness of the lattice, this energetic effect must become larger if we go to even smaller dot radii. It is these differences that we are interested in and that are to be studied more closely further below by comparing the effect of different lattices.

Figure 1(c) demonstrates the effect of the electron-hole interaction. The levels calculated with the interaction switched on are shifted up by 200 meV against the level scheme without interaction in order to make the differences become more clearly visible. The comparison reveals that although the electron-hole interaction is certainly of subordinate importance in the strong-confinement regime considered here, it is still strong enough to lead to a clearly recognizable overall distortion of the level scheme (the Coulomb interaction shows linear behavior in a $1/R^2$-plot) and that taking account of this interaction by an R-independent constant as done in Ref. 13 may thus be regarded as a fairly crude approximation.

Having illuminated its different parts, we are ready now to turn to the full problem of Eq. (9), taking into account all its components: electron, hole, and their mutual interaction. To begin with, we consider the case of hard-wall confinement potentials and focus our attention first on the ground-state level (see Fig. 2). It is evident from the comparison of this curve with the experimental data of Norris *et al.* that the

theoretical results disastrously fail to account for the experimental findings, a fact that according to Norris *et al.* might originate in the unjustified assumption of infinite potential barriers at the dot boundaries. This explanation is supported by the results of the theoretical work of Einevoll[17] who showed that when a finite barrier of $V_B = 500$ meV in a simple confinement potential is taken [$V(r) = V_B \Theta(r - R)$, with Θ for the step function], then the ground-state energies of an electron-hole pair in a CdS quantum dot can be nicely reproduced by the theoretical curve. Relying on the similarity of CdS and CdSe semiconductors, we repeat our calculation using for the electron in Eq. (12) the same confinement potential and the same barrier height as in Ref. 17 while keeping the infinite barrier for the hole. As can be seen from Fig. 2, we then find a curve that shows a remarkably good agreement with the experimental data, thus confirming the speculation of Norris *et al.* about the central role played by the finite barrier.

Introducing the same finite barrier likewise for the hole leads to a poorer fit for the ground state energies of Fig. 2, and, more importantly, considerably alters the level scheme for the higher excited states so that its good accordance with the experiment (discussed below) is almost completely destroyed. In conclusion, we can thus learn from experiment that while the hole in a CdSe quantum dot is effectively confined inside the dot boundaries, the electrons see but a finite barrier allowing them to tunnel into the nearby vicinity of the dot. This is shown in Fig. 3(a) where electron wave functions for different barrier heights in an $R = 13$ Å dot are compared. The barrier height of 500 meV is obviously quite low on account of which there is a comparatively high probability for finding the electron outside the volume defining the dot. It should be possible to explain both barriers — the effectively infinite barrier for the hole and the 500 meV barrier for the electron — with the mismatch of the band edges of the CdSe quantum dot and its surrounding material.

In Figs. 3(b) and 3(c), we plotted the hole energy levels and the corresponding oscillator strengths for a dot of $R = 13$ Å as a function of the barrier height. Through the potential $P(U_h)$ in Eq. (9), the changes of the electron wave function on varying the barrier height also affect the hole levels, though only to a negligibly small extent, which is not an unexpected result for such a strongly confined dot. The barrier has by contrast a major effect on the oscillator strengths: With the electron wave function varying as in Fig. 3(a) and the hole wave function wholly confined to the dot, the overall overlap of electron and hole wave functions and accordingly the oscillator strength must depend sensitively on the barrier height, as a glance at Fig. 3(c) will indeed confirm.

We make two concluding remarks relating to Fig. 2. (i) Also shown there is the energy for a transition from the highest hole level to the $2s$ electron level [from matrix (12)] for the 500-meV confinement potential. It lies more than 1 eV above the ground-state level and is therefore well separated from all the transitions to the $1s$ level. This may justify the drastic reduction of our basis (6) where we have taken up only the ground state of Eq. (12). (ii) To make them fit our theoretical curve, we had to shift the experimental points in Fig. 2 by 1.8 eV. This is then the gap energy required and

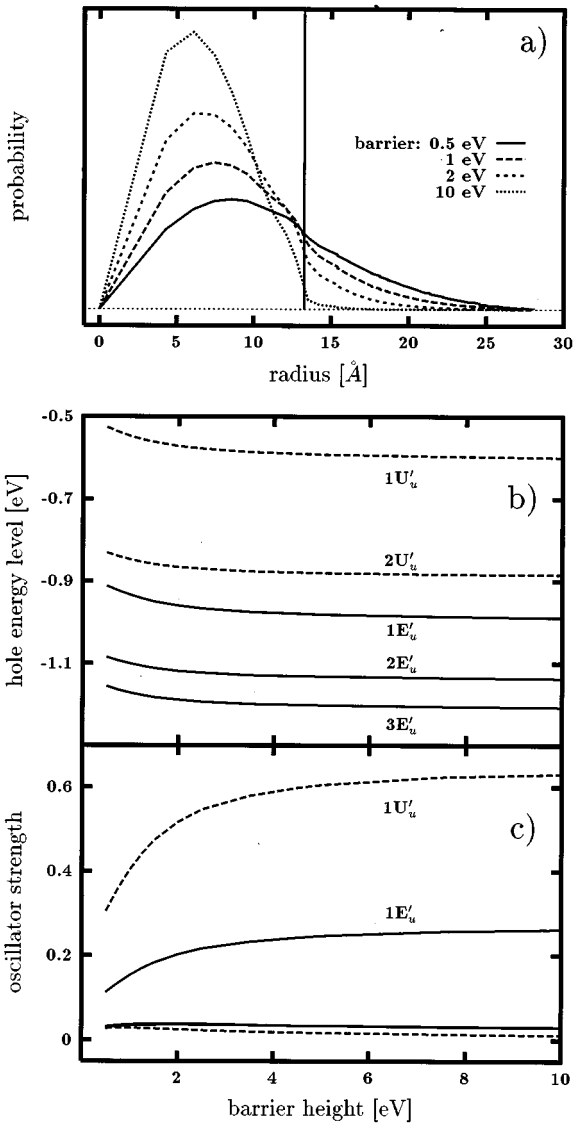

FIG. 3. Effect of a finite barrier for the electron at the dot boundary for a $R = 13$ Å dot. (a) Electron wave functions for various barrier heights. (b) Hole energy levels and (c) oscillator strengths as a function of barrier height.

should be compared with the literature value of 1.84 eV (Ref. 27).

We next turn our attention to the higher excited electron-hole states of Eq. (9). They are compared in Fig. 4(a) with the experimental results of Norris *et al.* Following these authors, we present our data in a somewhat unconventional form plotting relative transition energies (excited-state level minus ground-state level) versus the transition energy to the ground-state level. The ground-state energies are those from Fig. 2 plus 1.8 eV for the gap energy. The different levels are distinguished by the symmetry of the hole wave function with an additional integer counting upwards through the levels of the same symmetry. Only the levels involved in a transition of sufficient strength are shown ($f > f_T$).

Apart from the slight mismatch of the $3E'_u$ level, we find rather good agreement between experiment and theory. This is not surprising if one bears in mind that the decisive input parameters, the Luttinger parameters, have already proven

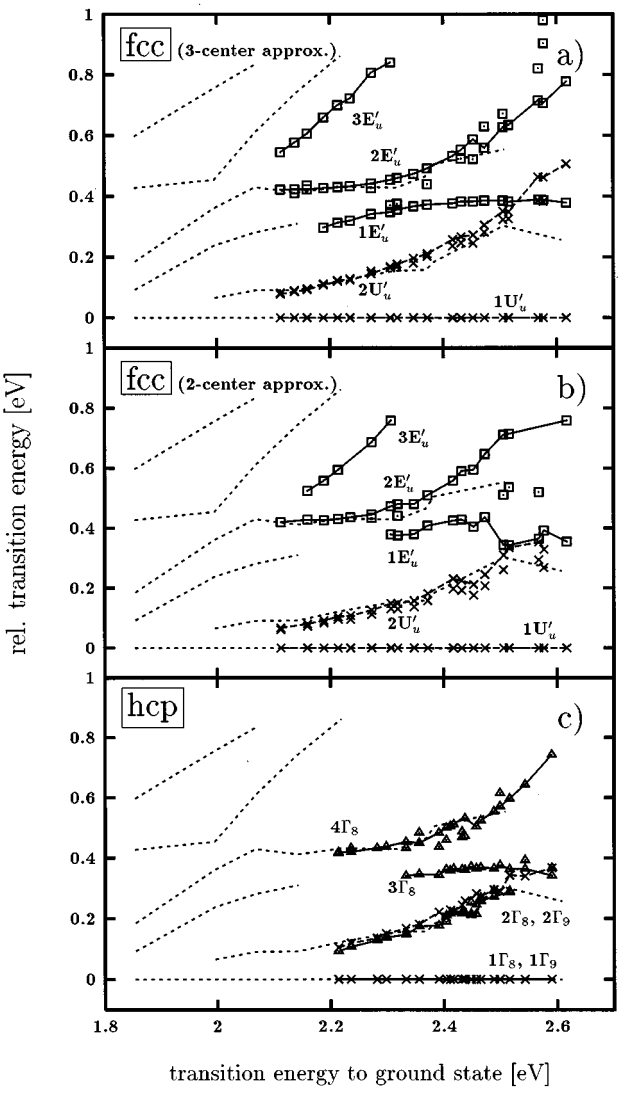

FIG. 4. Size dependence of higher excited levels of an electron-hole pair in a CdSe quantum dot and the effect of distinct lattice structures: a fcc lattice for the zinc blende (a), (b) and a hcp lattice for the wurtzite structure (c). The x axis gives the transition energy to ground-state level of Fig. 2, the y axis gives the excited state minus ground-state energy. Dashed lines connect experimental data of Norris *et al.* Shown are only levels where $f > f_T$. Dot size decreases with increasing energy on the x axis.

their quality in Ref. 13 as well as in the the work of Norris *et al.*, where a fairly satisfactory agreement was already found in the range below 2.2 eV using the five curves of Ekimov *et al.* displayed in Fig. 1(b). On closer inspection, though, the fit obtained there also reveals that the electron-hole interaction has not been taken into account properly. If the data are plotted as in Fig. 4, then the inclusion of the electron-hole interaction results in a common stretching of the energies along the x axis [cf. Fig. 1(c)], and hereby the fit considerably improves.

It is remarkable that these Luttinger parameters and the comparatively simple valence-band model we have used still do a good job in the range above 2.2 eV. Although the $1E'_u$ level is not seen in the experiment (due to limited resolution, perhaps), the calculated levels match the experimental data down to dots of only 13 Å radius (corresponding to a transition energy of 2.5 eV). Dots of this size contain only 177 atoms, so one would expect that the discreteness of the lattice would have a visible effect on the spectrum, something we have already observed in Fig. 1(b). Such an effect can best be seen by comparing the results for different discrete lattices.

This brings us to Figs. 4(b) and 4(c), the comparison of the solutions to Eq. (9) for a hcp and a fcc lattice. It demonstrates — and that is the central result of this investigation — that there is no significant difference between the level schemes for both lattices. Although a small splitting of the $2U'_u$ level into Γ_8 and Γ_9 is clearly recognizable, the overall pattern of the levels in Figs. 4(b) and 4(c) remains very much the same. We have pointed out earlier that in the case of the hcp lattice, it is neccessary to change from the three- to the two-center approximation, Eq. (16), so that $\underline{\underline{D}}(\vec{R}_{nn})$ in Eq. (13) can be determined from Eq. (15). Naturally, with the appropriate choice of the rotation matrices $\underline{\underline{R}}(\vec{R}_{nn})$, expression (15) can equally well be used for the fcc lattice [Fig. 4(b)]. We thereby ensure that the results for both lattices are compatible, i.e., based on the same approximation made for $pp\pi$ in Eq. (16). The effect of this latter approximation can be estimated by comparing Figs. 4(a) and 4(b). It turns out to be quite small, with only minor differences between the $1E'_u$ levels towards the smaller dots and hardly any differences between both the $2E'_u$ and the $2U'_u$ levels. Summarizing, we can thus conclude from Fig. 4 that in the dot-size range considered here, the discreteness of the lattice has virtually no effect on the energy levels of the dot, and that no matter what lattice type is assumed one always finds a fine agreement with the experimental data.

This is once more confirmed by Fig. 5, which displays the oscillator strengths for each of the three calculations of Fig. 4. To take account also of all levels with only small oscillator strengths [not necessarily shown in Figs. 4(b) and 4(c)], we have added all f values within a given interval and assigned it to the level with the highest f value [connected in Fig. 4 by lines]. Due to this coarse graining, the curves in 5(b) and 5(c) do not show as smooth a behavior as the curves in Fig. 5(a). But for this artifact, we see again that the three calculations vary in their results only by an insignificant amount.

Of course, one has to add the f values of the $1\Gamma_8$ and $1\Gamma_9$ levels to make them comparable to the strength of the $1U'_u$ level. The question then naturally arises if one can possibly distinguish the fcc from the hcp structure by using z-polarized light since such light excites only the Γ_8 level in the hcp lattice while being of no consequence in the fcc lattice. The answer to this question is negative: There is no such polarization effect. We find this from calculating the polarization degree for each level, i.e., the quotient of the f value in Eq. (20) to the corresponding f value for unpolarized light. They turn out to be roughly 2 for the $1\Gamma_8$ level and 1 for the $3\Gamma_8$ and $4\Gamma_8$ levels (to a good approximation size independent) so that one thus ends up with the same oscillator strengths as in Fig. 5(c).

In Figs. 4 and 5, we have only given the symmetries Γ_h of the hole wave functions while the overall symmetry of the electron-hole pair follows from Eq. (21). We see that T states for the O_h group split into A and E states when the D_{3h}

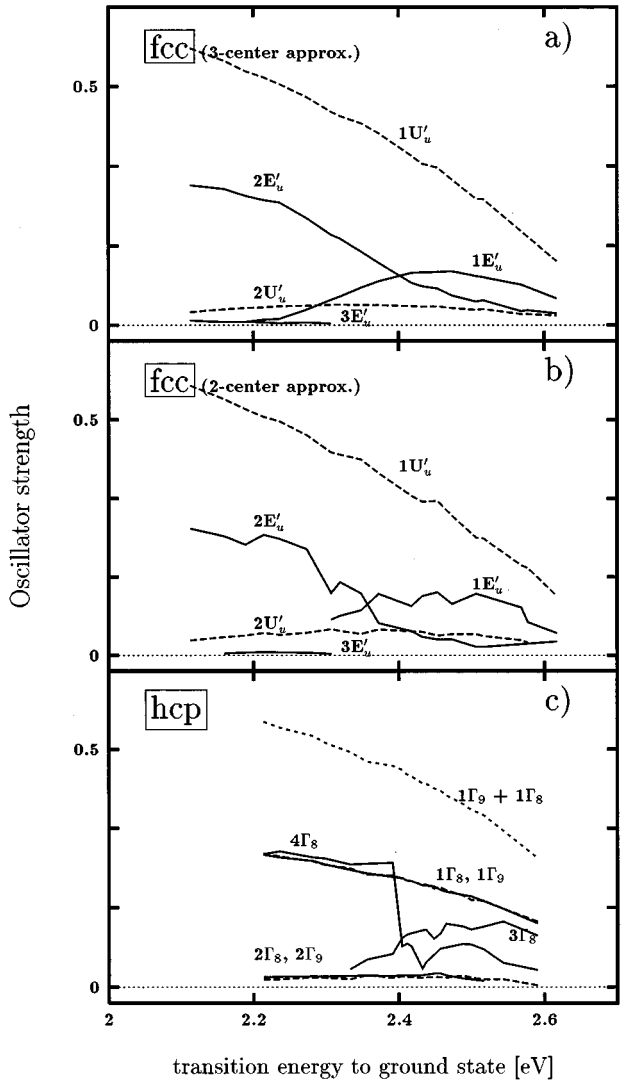

FIG. 5. Oscillator strengths for each of the three calculations in Fig. 4, plotted in the same way as in Fig. 4.

group is considered. Thus, the symmetry of the wurtzite structure explains why in the experiment of Shiang *et al.*,[21] which we mentioned in the introduction, only *A* and *E* but no *T* states have been observed. However, while in Ref. (21) splittings of the order of 100 meV have been measured, we by contrast see them lying in the range of a few meV only. With the results of Figs. 4 and 5, we can therefore rule out that the observed splittings stem from the wurtzite structure. This supports the concluding conjecture of Shiang *et al.* that the morphology of the crystallites is more likely to be responsible for the splittings.

Another implication of our findings concerns the EBOM method[22] used in Refs. 16–18 for calculating the energy levels of CdS and CdSe dots. This method is based on the assumption that a fcc lattice can always be used even though the correct lattice might be different. Assuming the CdSe system to be prototypical for similar quantum dots, we can learn from our results that the error produced by this approximation is indeed negligible. Another fundamental assumption usually made for such tight-binding models is that it suffices to include only the bands lying nearest to the band gap. This is only a good approximation as long as the band states near the zone edge have but a minor effect on the final results. If this is the case, then the shape of the first Brillouin zone (and thus the lattice structure in real space) should likewise not be significant. We hence see the connection between the validity of the restriction to only a subset of bands, on the one hand, and the requirement that the lattice structure should not be important, on the other. Having shown the latter to be true, we thus have confirmed the first statement also.

Another aspect is finally noteworthy. If the energy levels are roughly the same for the hcp as for the fcc lattice, then it also should not matter if an even simpler effective lattice, like, e.g. the simple cubic lattice, is taken. This points to a way of how to further simplify such EBOM models.

IV. CONCLUSION

We have studied the effect that a change from a zinc blende to a wurtzite structure has on the energy levels of a CdSe quantum dot. This has been done with the help of an ordinary tight-binding model in which the electron and hole transfer matrix elements between neighboring lattice sites are derived from the shape of the bands near $\vec{k}=0$ of the zinc-blende CdSe band structure. The same effective σ and π bonds have been used in both a hcp and a fcc lattice to model CdSe in the wurtzite and the zinc-blende structure, respectively. Within the limits of this model, we see no significant differences between both crystal structures in the dot size range considered here: the curves of both energy levels and oscillator strengths over dot radius are very similar in either structure down to dots of $R=13$ Å, thus suggesting that the relevant band states come from a $\vec{k}$ region where the bands have a form that is not specific for the shape of the Brillouin zone. It is therefore unlikely that a calculation based on more subtle band approximations for both the wurtzite and zinc-blende form of CdSe will come to a dramatically different result. This also means that ignoring the Brillouin zones altogether, i.e., choosing a continuum approach, should work equally well.

For a whole range of dot radii, both calculations, for the wurtzite and the zinc-blende structure, yield the same good agreement with the absorption data of Norris *et al.*; and this with respect to both the ground-state level as well as levels of the higher excited states. For the larger dots, a satisfactory fit to the theoretical curves of Ekimov has already been obtained by Norris *et al.*, while the underlying valence-band approximation has now been shown to work equally well for the smaller dots. A finite barrier for the electron was found to be the key for interpreting the as yet unexplained ground-state data. Taken together, we have thus provided a consistent unified description of the whole series of electron-hole states observed by Norris *et al.* The nice agreement obtained is particularly satisfying since it is achieved using the gap energy as the only fitting parameter.

This good agreement is completely destroyed on introducing a finite barrier for the hole too. So the experiment reveals that on account of their different barriers, the electron wave function is spread far beyond the dot's boundary, while the hole wave function is wholly confined inside the dot. Consequently, the overlap between both wave functions, and

thus also the oscillator strengths depend sensitively on the electron barrier height. In this context, it is interesting to think of an experiment in which this barrier dependence of the oscillator strengths is used to ''switch off'' certain levels in the absorption spectrum.

Our results also help to establish that the large splittings of the *T* states observed in the experiment of Shiang *et al.* cannot originate in the wurtzite structure. They must arise therefore as a result of the nanocrystal shape and surface. Although there are already a few works dealing with shape effects in quantum dots,[28] attention has mainly been paid to simple boundary shapes, such as a cubic[30] or cylindrical[29] ones. Still missing are calculations considering more realistic but also more complicated boundary shapes such as, for example, one with well-defined facets, as proposed in Ref. 21. This is a question which likewise can be studied within the framework of the tight-binding model used here.

ACKNOWLEDGMENTS

I thank Professor K.P. Jain for his hospitality and all the interesting discussions we have had during my stay at the Indian Institute of Technology where this work was started. Also, I am indebted to Professor Sir Roger J. Elliott for many stimulating discussions and critical comments on the manuscript. I finally gratefully acknowledge the financial support received for the project No. CI1*-CT94-0090 from the European Community under which this work was performed.

[1] Recently reviewed by U. Woggon, and S.V. Gaponenko, Phys. Status Solidi B **189**, 285 (1995); Y. Kanemitsu, Phys. Rep. **263**, 3 (1995); A.D. Yoffe, Adv. Phys. **42**, 173 (1993).
[2] Al.L. Efros and A.L. Efros, Sov. Phys. Semicond. **16**, 772 (1982).
[3] L.E. Brus, J. Chem. Phys. **80**, 4403 (1984).
[4] Recently reviewed by G.C. John, V.A. Singh, Phys. Rep. **263**(2), 94 (1995).
[5] S.V. Nair, S. Sinha, and K.C. Rustagi, Phys. Rev. B **35**, 4098 (1987).
[6] Y. Kayanuma, Phys. Rev. B **38**, 9797 (1988).
[7] G.W. Bryant, Phys. Rev. B **37**, 8763 (1988).
[8] A.I. Ekimov, Al.L. Efros, M.G. Ivanov, A.A. Onushchenko, and S.K. Shumilov, Solid State Commun. **69**, 565 (1989).
[9] Y.Z. Hu, S.W. Koch, M. Lindberg, N. Peyghambarian, E.L. Pollock, and F.F. Abraham, Phys. Rev. Lett. **64**, 1805 (1990).
[10] K.D. Zhu, S.W. Gu, Phys. Lett. A **172**, 296 (1993); G. Li, S.V. Branis, K.K. Bajaj, Phys. Rev. B **47**, 15735 (1993); M. Elsaid J. Phys. (France) I **5**, 1027 (1995); M. Elsaid, Phys. Status Solidi B **193**, 105 (1996).
[11] G.W. Wen, J.Y. Lin, H.X. Jiang, Z. Chen, Phys. Rev. B **52**, 5913 (1995).
[12] Al.L. Efros and A.V. Rodina, Solid State Commun. **72**, 645 (1989); G.B. Grigoryan, E.M. Kazaryan, Al.L. Efros, and T.V. Yazeva, Fiz. Tverd. Tela (Leningrad) **12**, 103 (1989) [Sov. Phys. Solid State **32**, 1031 (1990)]; J.B. Xia, Phys. Rev. B **40**, 8500 (1989).
[13] A.I. Ekimov *et al.*, J. Opt. Soc. Am. B **10**, 100 (1993).
[14] Y. Wang, A. Suna, W. Mahler, and R. Kasowski, J. Chem. Phys. **87**, 7315 (1987).
[15] P.E. Lippens and M. Lannoo, Phys. Rev. B **39**, 10 935 (1989); **41**, 6079 (1990).
[16] G.T. Einevoll and Y.C. Chang, Phys. Rev. B **40**, 9683 (1989).
[17] G.T. Einevoll, Phys. Rev. B **45**, 3410 (1991).
[18] S.V. Nair, L.M. Ramaniah, K.C. Rustagi, Phys. Rev. **45**, 5969 (1992); S.V. Nair, L.M. Ramaniah, K.C. Rustagi, Phys. Rev. Lett. **68**, 893 (1992); L. Ramaniah, S.V. Nair, Phys. Rev. **47**, 7132 (1993).
[19] Y. Kayanuma and H. Momiji, Phys. Rev. B **41**, 10 261 (1990).
[20] D.J. Norris, A. Sacra, C.B. Murray, and M.G. Bawendi, Phys. Rev. Lett. **72**, 2612 (1994).
[21] J.J. Shiang, A.V. Kadavanich, R.K. Grubbs, and A.P. Alivisatos, J. Phys. Chem. **99**, 17 417 (1995).
[22] Y.C. Chang, Phys. Rev. B **37**, 8215 (1988).
[23] G.T. Einevoll, D.S. Citrin, and Y.C. Chang, Phys. Rev. B **44**, 8068 (1991).
[24] J.C. Slater and G.F. Koster, Phys. Rev. **94**, 1498 (1954).
[25] J.M. Luttinger and W. Kohn, Phys. Rev. **97**, 869 (1955); J.M. Luttinger, Phys. Rev. **4**, 1030 (1956).
[26] H.H. von Grünberg, and H. Gabriel, J. Chem. Phys. **103**, 6040 (1995).
[27] *Semiconductors Physics of Group IV Elements and III-V Compounds*, edited by K. H. Hellwege, Landolt-Börnstein, New-Series, Group III, Vol. 17, Pt. a (Springer, Heidelberg, 1982), Chap 3.11.
[28] M.E. Schmidt, S.A. Blanton, M.A. Hines, and P. Guyot-Sionnest, Phys. Rev. B **53**, 12 629 (1996).
[29] S. Legoff, B. Stebe, Phys. Rev. B **47**, 1383 (1993).
[30] R. Romestain and G. Fishman, Phys. Rev. B **49**, 1774 (1994).